Deuterium inventory in the full tungsten divertor of ASDEX Upgrade

K. Sugiyama, M. Mayer, V. Rohde, M. Balden, Th. Dürbeck, A. Herrmann, S. Lindig, A. Wiltner, H.W. Müller, R. Neu and the ASDEX Upgrade team

Max-Planck-Institut für Plasmaphysik, EURATOM Association, Boltzmannstrasse 2, D-85748 Garching, Germany

E-mail: kazuyoshi.sugiyama@ipp.mpg.de

Abstract. The deuterium inventory in tungsten-coated divertor tiles used during the first full-tungsten plasma-facing wall phase of ASDEX Upgrade was measured by various analysis methods. The D inventory in the inner divertor was still dominated by codeposition with residual carbon, whereas it was dominated by trapping in the thicker vacuum plasma sprayed tungsten layers at the outer divertor. The total inventory in the divertor area decreased by a factor of 5 ~ 10 compared to the period of carbon-dominated plasma-facing wall.

PACS numbers: 28.52.Fa, 52.40.Hf, 52.55.Fa

1. Introduction

The material choice of the plasma-facing components for future fusion devices is governed by boundary conditions raised from various objectives such as erosion lifetime, neutron irradiation, thermo-mechanical issues and radiative cooling / dilution of the plasma. From these considerations, the current design of ITER plasma-facing components envisages using several different armour materials depending on the operational requirements. Beryllium (Be) is the primary candidate for the main chamber wall material, whereas tungsten (W) is selected for the divertor armor, except for the strike point areas where carbon fibre composite is designated as armor material [1]. However, there is some concern that this selection of wall materials can cause unacceptably high tritium inventories due to the high erosion yields of Be and C, and succeeding codeposition of these materials with tritium. This can strongly affect ITER operation especially in the D-T phase because periodic tritium removal will be required before the in-vessel tritium inventory reaches its administrative limit of currently 700 g [2]. From this viewpoint, the feasibility of a full high-Z wall in the later phase of ITER is being discussed for the reduction of tritium inventory and prolongation of wall lifetime [3-5].

In ASDEX Upgrade (AUG), the stepwise transition of the plasma-facing wall material from carbon to tungsten has been proceeded since 1999 [6]. This offered the unique possibility to investigate the influence of the wall material on deuterium (D) inventory as well as the compatibility of W as a plasma-facing material. The area of the W surface was increased step by step. As last component, the divertor targets were finally replaced by W-coated tiles after the 2005/2006 campaign, and AUG operated with a fully W-covered plasma-facing wall and without boronization during the 2007 campaign. After the campaign, a set of divertor tiles was removed from the vacuum vessel in order to investigate the D inventory in the W divertor by various post-mortem analysis methods. In this article, the results of D retention analysis are overviewed and its characteristics are discussed.

2. Experimental details

2.1. Sample specification and plasma operation history

During the 2007 campaign the divertor IIc configuration was used. A Schematic view of the divertor cross-section is shown in figure 1 (a). The design of the divertor was slightly changed from the previous divertor IIb configuration in order to allow failsafe W cooling. All tiles consisted of W-coated fine grain graphite. The thickness of the W coating was 3 ~ 5 μm prepared by physical vapor deposition (PVD), except for the outer target (tile 1) where a 200 μm thick W coating deposited by vacuum plasma spraying (VPS) was used (shown in figure 1 (b)). A detailed description regarding the development of W coatings for AUG is available in [7-9]. Langmuir probes installed in the outer target area (shown in figure 1 (b), (c)) were measured as well as W-coated tiles. The probes consisted of polycrystalline (PC) bulk W, which allows a direct comparison of the D inventory in PC-W and VPS-W.

The total discharge time with lower X-point divertor configuration was 2620 s during the 2007 campaign. The inner and outer divertor strike points were mostly located on tiles 4 and 1, respectively, as shown in figure 2 (a). According to the Langmuir probe data, the accumulated D fluence during the whole campaign in the outer divertor target area was of the order of 10^{25} /m^2.

No boronizations were performed in the 2007 campaign, and no hydrogen (H) discharges at the end of the campaign were carried out.

2.2. Surface temperature history

The surface temperature of the divertor targets in ASDEX Upgrade is routinely measured with fast IR-line cameras [10,11]. The surface temperature distribution of the inner and outer strike point tiles for all plasma shots in the 2007 campaign is shown in figure 3. The surface temperature reached about 1000 K during ELM's, but only for short time intervals of a few ms in a few discharges. Typically the maximum surface temperature stayed below about 800 K even during ELMs. The maximum surface temperature averaged over 50 ms usually stayed below 500-600 K at the inner strike point, while the outer strike point got hotter and reached a maximum of about 700 K for more than 50 ms. The mean tile surface temperature during the whole discharge period was 360 K at the outer and 340 K at the inner strike point. The mean tile temperature during individual discharges was always below about 490 K at the outer and about 430 K at the inner strike point. These surface temperatures are considerably lower than observed with the carbon divertor in the discharge campaign 2002/2003, where temperature excursions during ELMs up to 1800 K and mean tile temperatures during single discharges up to 600 K were observed [12]. One reason for this is the change of the divertor geometry from an ideal to a polygonal surface in 2004. The polygonal approximation of the toroidal divertor contour results in a temperature variation across a single target tile of up to 20 % [13].

2.3. Post-mortem analyses

The amount of retained D in the surface was measured by nuclear reaction analysis (NRA) using the D(^{3}He, p)^{4}He reaction. The poloidal distribution was obtained by measuring the surface along the poloidal direction at 1 cm step using 2.5 MeV ^{3}He$^+$ incident energy. This allows detecting the amount of D retained within a depth of ~ 3 μm. At this incident ^{3}He$^+$ energy, ^{12}C is simultaneously detectable

by collecting protons from the $^{12}C(^{3}He, p)^{14}N$ reaction, and its information depth is about 0.6 μm. NRA using $^{3}He^{+}$ at different incident energies was applied at some specific points in order to determine the D depth profile quantitatively [14]. For this case, the energy of ^{3}He was varied from 0.69 to 4.0 MeV, which allows measuring the D depth profile until a depth of about 6 μm [15]. The SIMNRA program [16] was used for the data evaluation.

Depth profiles of D, C and W were measured by secondary ion mass spectrometry (SIMS) using 10 keV Ar^{+} as primary ion beam. The SIMS depth scale was calibrated by measuring the depth of the sputter crater with a profiler after the measurement. SIMS allows deeper measurements beyond 6 μm. In addition, the morphology of tile surface was investigated by scanning electron microscopy (SEM) combined with focused ion beam (FIB) cross-sectioning.

After those surface analyses, the total amount of retained D including the amount trapped in the bulk was finally determined by thermal desorption spectroscopy (TDS) in the TESS set-up [17] at IPP-Garching. TDS samples were prepared by cutting out from each tile surface with the dimension of 10 mm × 20 mm × 2 mm, except the Langmuir probes which were investigated without cutting. The sample was heated from room temperature (RT) to 1200 K with a heating ramp of ~ 0.5 K/s (kept at 1200 K for half an hour) at a background pressure of ~ 10^{-7} Pa. Desorbed gases were analyzed by a quadrupole mass spectrometer (QMS).

3. Results

The poloidal D distribution obtained by NRA and TDS is shown in figure 2 (b), and the C distribution obtained by NRA is given in figure 2 (c). The s-coordinate used as the poloidal scale starts at the upper edge of tile 6A and then follows the divertor surface until the right edge of tile 3B (each tile No. is shown in figure 1).

As can be seen in figure 2 (c), there was still a non-negligible carbon deposition even after eliminating all carbon plasma-facing surfaces. According to the ion beam analysis result, in total about 1.3 g deposited carbon were measured in the divertor and in remote areas, of which 0.85 g were found on the inner divertor tiles, 0.13 g on the outer divertor tiles, and 0.28 g in remote areas [18]. Although some possible carbon sources in the W surface environment were suggested, it is not fully understood yet. On the surface of the inner divertor throat (tile 6A and 6B), many arc tracks were observed, which resulted in a partial removal of the PVD-W layer and some carbon erosion from the graphite substrate [19]. Some of the carbon deposition on tiles 6A and 6B can be attributed to this carbon erosion and nearby redeposition on those tiles. There was a thick carbon deposited layer (up to around 1 μm) with laminar structure on the inner private flux region (tile 4: just below the inner strike point area) as shown in figure 4.

As generally observed in tokamaks, the C deposition on outer divertor tiles was much smaller than on inner divertor tiles. Again, the D distribution measured by NRA (within 3 μm) seems to be correlated with the distribution of C deposition on the top of W surface as well as in the inner divertor region. One can find that the amount of C on the outer target tile (tile 1) was somewhat higher than in other parts of the outer divertor. This is probably due to the rougher surface of the VPS-W layer than that of PVD-W layer. There are many pores and valleys on the VPS-W layer where “plasma-shadowed areas” are formed during a discharge. From SEM observation, some local C depositions were found in such pores and valleys.

TDS spectra of hydrogen isotope molecules obtained from each W layer and Langmuir probes are shown in figure 5. Note that the temperature for Langmuir probe samples is given as "surface temperature" indicating the temperature measured by a thermocouple, which was attached to the probe surface during the measurement. It can be expected that the temperature increase inside of the probe bulk delayed slightly compared to the surface because the probe was massive (~ 5 mm thickness), meaning the temperature in the bulk could be somewhat lower than the "surface temperature". Deuterium was mainly released as HD (mass = 3) and D_2 (mass = 4) molecules, and some samples especially from inner divertor tiles showed relatively large amounts of D released as hydrocarbon species. Each D_2 desorption spectrum likely consisted of 6 ~ 7 peaks fitted by Gaussian functions as a first approximation, and the contribution of each peak varied depending on the poloidal location. According to laboratory investigations about D_2 desorption from W, 3 major desorption peaks have been confirmed under this kind of experimental conditions (details will be discussed in the next section). This implies that the spectrum from AUG samples consists of not only W-related but also something other (probably, C-related desorption) peaks. The result shown as "TDS" in figure 2 (b) was obtained by integrating the TDS spectra. It should be noted that the amount of D determined by TDS was higher than the result obtained by NRA by a factor of 2 ~ 3 in the case of VPS-W tiles, whereas TDS and NRA results agreed well in the case of PVD-W tiles, where the W-layer was thinner. One can find that non-negligible H_2 (mass = 2) was released from the samples in spite of no H discharges. However, each H_2 profile and the amount of H did not vary so much with the poloidal position or the amount of C deposition on the surface, which implies that the release of H_2 is mostly due to the contribution of H retained in the sample intrinsically.

Figure 2 (d) shows the D retention in Langmuir probes together with the results of VPS-W tiles. From the NRA results, the amount of D retained in the surface of Langmuir probes was roughly one order of magnitude less than that of VPS-W tile. However, the TDS results were at a comparable level with that of VPS-W tiles (see figure 5 (b), (c)).

4. Discussion

4.1. C distribution on W surface

The lateral C deposition distribution in the full-W divertor was qualitatively different from that observed previously in the carbon divertor. In the carbon divertor the thickest deposition was always observed around the strike point area, while in the W divertor the thickest C deposition was observed below the inner strike point in the private flux region. The ^{13}C injection experiments performed in TEXTOR showed that the C deposition efficiency on graphite surface is higher than that on W surface by a factor of 5 ~ 10 because the kinetic reflection coefficient of C or D from W is higher than from graphite surface, which could enhance re-sputtering of carbon deposition on W surface [20, 21]. Carbon deposited on the strike point area, where it was exposed to high flux plasma, could be easily re-eroded and further transported, whereas C deposited on the private flux region could stay without re-erosion due to the lower plasma influx there. In the inner divertor, the amount of retained D determined by TDS agreed with NRA results, and its distribution was very similar to C distribution, indicating that the D retention is well associated with the C deposition on the top of the W surface.

4.2. D retention in different W materials

While for the thin 3 μm PVD coatings the TDS and NRA results agreed well, the TDS results were higher than NRA in the case of thick VPS-W coated tiles and PC-W. Figure 6 shows depth profiles of D and C obtained by SIMS together with D depth profiles determined by NRA. As can be seen in the figures, the D profiles from SIMS and NRA showed excellent agreement. In the PVD-W layer, the D profile decreased quickly with depth, and the measured D concentration in the graphite substrate was at least 4 orders of magnitude less compared to the concentration at the top surface. This value is an upper boundary for the concentration of D in the bulk C due to unavoidable tail in the SIMS measurements by recoil implantation and roughness effects. In figure 6 (b), the profile obtained from the private flux region (s ~ 0.5 m) shows a high D concentration with ~ 30 at. % on the top surface within ~ 1μm. This is due to the C deposited layer (see Fig. 4), which confirms that a-C:D layers with a ratio of D/C ~ 0.4 are formed. Since D diffusion in graphite is very small (except the migration via pores), D accumulation in the substrate was limited. Therefore, the D inventory in PVD-W tiles was dominated by codeposition with C on the surface and retention in PVD-W layer, especially in the near surface area, and most of the D was retained within the detectable range of NRA (< 1μm C deposition + 3 ~ 4 μm PVD-W layer), which is the reason that TDS and NRA results showed good agreement.

On the other hand, D profile in VPS-W layer decreased more gradual than that in PVD-W layer (figure 6 (c)). As can be seen in figure 7, the VPS-W layer shows a much more porous structure with fissures and voids, compared to PVD-W or PC-W. In such a structure, it could be easier for D to pass deeper into the layer, and such pores can act as D trapping sites. Moreover, since D diffusion in W is much faster than in graphite, the amount of D accumulated over the whole layer (200 μm, meaning further beyond the detectable range of NRA) was consequently comparable with the amount of D retained in near surface area, leading to a larger amount of D detected by TDS than by NRA for the VPS-W layer.

Figure 6 (d) shows D depth profile in PC-W Langmuir probe together with that in VPS-W from identical poloidal location for comparison. As found in NRA result, D concentration in PC-W was roughly one order of magnitude smaller than that in VPS-W within the top 3 μm. It decreased quickly with depth, both in PC-W and PVD-W. However, the total amount of D determined by TDS leaped upward from the NRA result by about 2 orders of magnitude (figure 2 (d)). This means that a significant amount of D was accumulated in the W bulk despite the low D concentration ($\leq 10^{-2}$ at.%). This implies that D diffused into the bulk until a depth of a few millimeters, otherwise the large amount of D determined by TDS cannot be explained.

As can be seen from figure 6, the C depth profile has a very similar shape as the D depth profile in the W layers. Carbon may be present as impurity in the W layers due to the layer deposition procedure at a level up to a few percent, or it may penetrate into VPS-W through the network of open porosity as hydrocarbon radical with low sticking probability. Therefore, the SIMS profiles suggest that C played a role for D trapping not only in layers at the inner divertor, but also for the deep penetration in the W layers.

The fluence dependences of the AUG results and literature data [22-25] are compared in figure 8. The AUG data plotted here are from VPS-W and PC-W (Langmuir probes) samples. One can find that the AUG results are on the extrapolation of the laboratory data that were obtained at RT, but don't fit perfectly to the results obtained at elevated temperatures despite the fact that the outer divertor was heated to above 400 K during a discharge. Recent laboratory investigations suggested different trapping sites in PC-W, i.e. (1) weak trapping in dislocations / grain boundaries with a trapping energy: E_{trap} of 0.6 - 0.9 eV, (2) trapping in vacancies / bubbles with E_{trap} ~ 1.2 - 1.6 eV and (3) chemisorption on the inner surface of a void with a high trapping energy (E_{trap} ~ 1.8 - 2.0 eV)

[22,23,26-28]. In the case of PC-W, D is mainly trapped in (1) and (2) sites under RT irradiation, while trapping by (3) sites becomes dominant under higher temperature irradiation conditions. As can be seen in figure 5 (c), the contributions of trapping sites (1) and (2) are relatively small and the high temperature peak is more prominent. Such desorption profile qualitatively agrees to laboratory results performed at elevated temperature conditions, but the amount of retained D was higher than that expected from such laboratory results. As already mentioned above, a possible explanation could be deep diffusion of D in the Langmuir probe. According to Frauenfelder [29] and Zakharov et al [30], D diffusivity in W reaches ~ 10^{-5} m/s at 800 K. Although the mean surface temperature on the outer divertor tiles was always below 500 K during a whole discharge, the surface occasionally heated up to about 800 K for more than 50 ms due to high heat load events such as ELMs (see figure 3). In addition, since Langmuir probes were not operated at the floating potential, the load to the probe from plasma was larger than that to normal tiles. And the additional electrical isolation hinders the cooling of the probe. It is, therefore, expected that each Langmuir probe was heated higher than surrounding tiles. Transient heat loads can cause temperature gradients between surface and bulk, which can be a driving force for D diffusion. Note that the Langmuir probe was made of technical W, meaning that the quality, i.e. impurity level, crystallinity, number of cracks etc., could not be as good as well-prepared W used in laboratory experiments, which might increase the number of trapping sites in the bulk. Further investigation of D in massive PC-W exposed to the divertor plasma is continued by using the AUG divertor manipulator system [31], which is planed to be performed in upcoming campaigns.

According to Golubeva et al. [25], the D_2 desorption profile of VPS-W was qualitatively different from PC-W, namely, a large fraction of D was trapped in high energy trapping sites already at RT irradiation. This is reasonable because the concentration of voids in VPS-W is intrinsically higher than that in PC-W or PVD-W. In VPS-W at elevated temperatures the contribution of the low temperature peaks becomes smaller with increasing irradiation temperature, whereas the high temperature peak remains unchanged. The amount of retained D irradiated at 473 K was roughly half of that irradiated at RT. Although the D_2 desorption profile of AUG VPS-W shows a similar tendency, the total amount of retained D was slightly higher than that expected from the laboratory results. On the other hand, it should be kept in mind that C deposition / impurity could influence the D trapping in VPS-W, and D retention in VPS-W strongly depends on the microstructure of the VPS coating, such as porosity or surface roughness [32].

4.3. Surface modifications of plasma-exposed tungsten

The plasma-exposed surface of the PC-W Langmuir probe was investigated by SEM combined with FIB cross-sectioning and X-ray spectroscopy.

The back side of the Langmuir probe was machined in the same way as the front side. The feature observable on the back side were taken as representative for the effect of machining the probes. The technical surface exhibits many different features, mainly grinding grooves (figure 9(a)) and pores just below the surface by smearing material over unevenness. This variation of surface features on a technical surface strongly hinders the interpretation of the observed features in respect of plasma exposure. Nevertheless, the most obvious effect of the plasma exposure is the smoothing of the surface topography (figure 9(b)). The smoothed surface leads to the impression that many elongated structures on the surface are aligned, as it is typical for surface with strong erosion/re-deposition

morphology [33]. From the composition of those surfaces, it can be excluded that re-deposited carbon/boron layers are responsible for these topography.

Some of surface uprisings show blister-like feature (figure 9(b)). However, cross-sectioning shows unquestionably that these features are not typical blister with a thin cap above a larger cavity as observed for He bombardment on many metals [34]. They are also different compared to the recently observed features on W after high flux D plasma exposure, which were described by irregular shaped surface structures with corresponding cavities and cracks underneath [35,36]. Many of these uprisings have a foam-like morphology (figure 9(c)). Their chemical composition was checked to be W. Similar foam-like structures were previously observed created by He bombardment at elevated temperature [37,38]. It is unclear how these localized foamy uprisings are produced.

No correlation between observed pores and cavities with surface structure due to plasma exposure could be drawn. Beside the natural pores in bulk material, pores due to the strong deformation of the surface during the machining are observed, which could easily misinterpret as cavities belonging to blisters (figure 9(d)).

Some concern has been expressed for blisters due to the small thermal conductivity of the blister cap, which can result in melting of the W and enhanced erosion. According to the present investigation, this concern seems unjustified for the surface modifications observed at AUG. However, ITER will reach much higher fluences as can be reached in AUG, and the surface structure at ITER fluences is difficult to predict from current knowledge.

Some blister-like structures were observed on W-coated tiles as well [39]. However, since these W layers have a high surface roughness and contain a substantial number of cavities and cracks already from the beginning, it is not clear that the formation of such structure was caused by the plasma exposure.

4.4. Evolution of the D inventory in the ASDEX Upgrade divertor

The D inventory in the divertor from the 2002/2003 campaign (C-dominated machine) until the 2007 campaign (full W wall) is summarized in figure 10. The D inventory in the inner divertor and in remote areas has decreased by reducing the area of carbon plasma-facing wall components, while the amount of D in the outer divertor remained almost constant. Deuterium inventory due to the codeposition with C or B was more prominent [12]. Therefore, the removal of carbon and no boronizations can drastically decrease the D inventory. The outer divertor area was always erosion dominated, and the decrease of C did not influence so strongly on the D inventory in the outer divertor. Besides, the D retention in thicker VPS-W layers became dominant, which led to a slight increase in the D inventory in the outer divertor area. As a consequence, the total D inventory in the divertor has decreased by a factor of 5 ~ 10 compared to the period with carbon-dominated plasma-facing components.

5. Concluding remarks

The D inventory in the fully W-covered ASDEX Upgrade divertor tiles was investigated by nuclear reaction analysis (NRA), thermal desorption spectroscopy (TDS) and secondary ion mass spectrometry (SIMS) after the 2007 discharge campaign. The D inventory in the inner divertor dropped drastically due to the reduction of carbon deposition, as compared to the carbon-dominated

machine. Nevertheless, even after eliminating all carbon plasma-facing surfaces, there was still a non-negligible carbon deposition forming a-C:D layers especially in the private flux region. Depth profiles of C and D in W layers showed a similar behaviour, implying not only residual C deposition but also C impurities in the W layers play a role for D retention. The total amount of D in the outer divertor did not change strongly in the 2007 campaign compared to previous campaigns, because the outer divertor area was always erosion dominated, i.e. the influence of the decrease of C was small. For thick vacuum plasma-sprayed W coatings (VPS-W) and bulk polycrystalline W (PC-W), the amount of retained D measured by TDS was always higher than that measured by NRA within the top 3 μm. This result indicates that diffusion and accumulation in the bulk plays an important role for the D inventory. The D depth profiles in VPS-W and PC-W were very different due to the different material structure, but the total amounts were comparable. In PC-W surface modifications due to the plasma exposure were observed. These modifications appeared to be blister-like structures, but they had a foam-like morphology without blister cap, which was different from classical blister structure reported by laboratory experiments. The labeling “blister”, as used by some authors, is therefore misleading and should be avoided in this case. The total D inventory in the divertor area decreased by a factor of 5 ~ 10 compared to the carbon dominated machine, which encourages that a full-W plasma-facing wall could be a feasible solution from the viewpoint of reduction of in-vessel tritium inventory in next step fusion reactors.

Acknowledgements

The technical assistance by J. Dorner and M. Fußeder is gratefully acknowledged. One of authors, K. Sugiyama would thank the support by JSPS Postdoctoral Fellowship for research abroad.

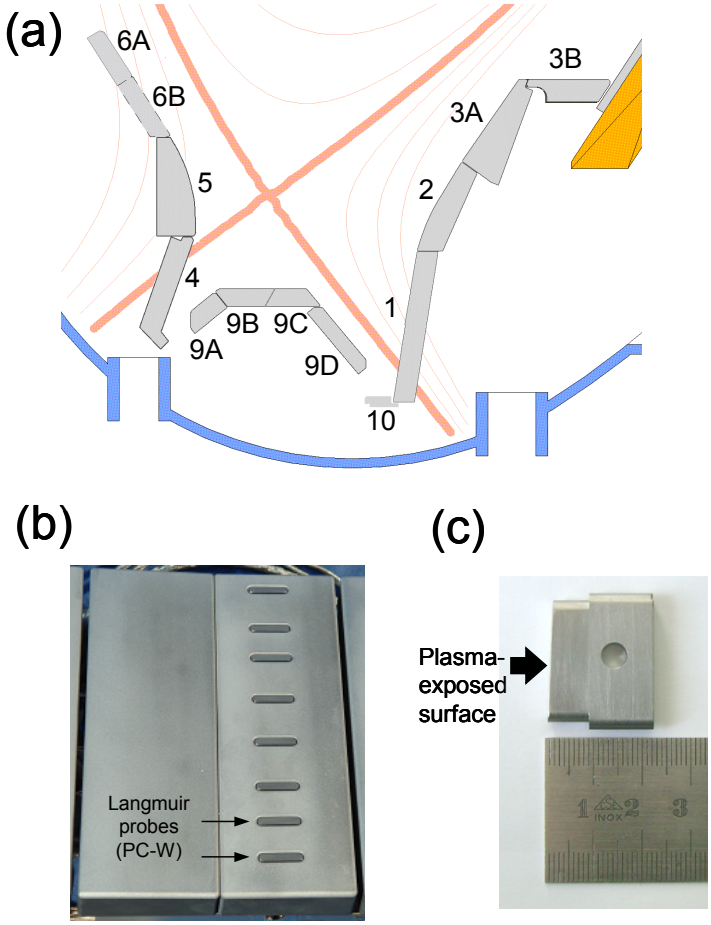

Figure 1. (a) Cross-sectional view of the ASDEX Upgrade divertor used during the 2007 campaign. All tiles consist of PVD-W coated (3- 4 µm) graphite, except for the outer target tile (tile 1) which is VPS-W coated (200 µm) graphite. (b) Picture of tile 1 with Langmuir probes installed in the outer divertor target area. (c) Picture of a Langmuir probe made of polycrystalline bulk W.

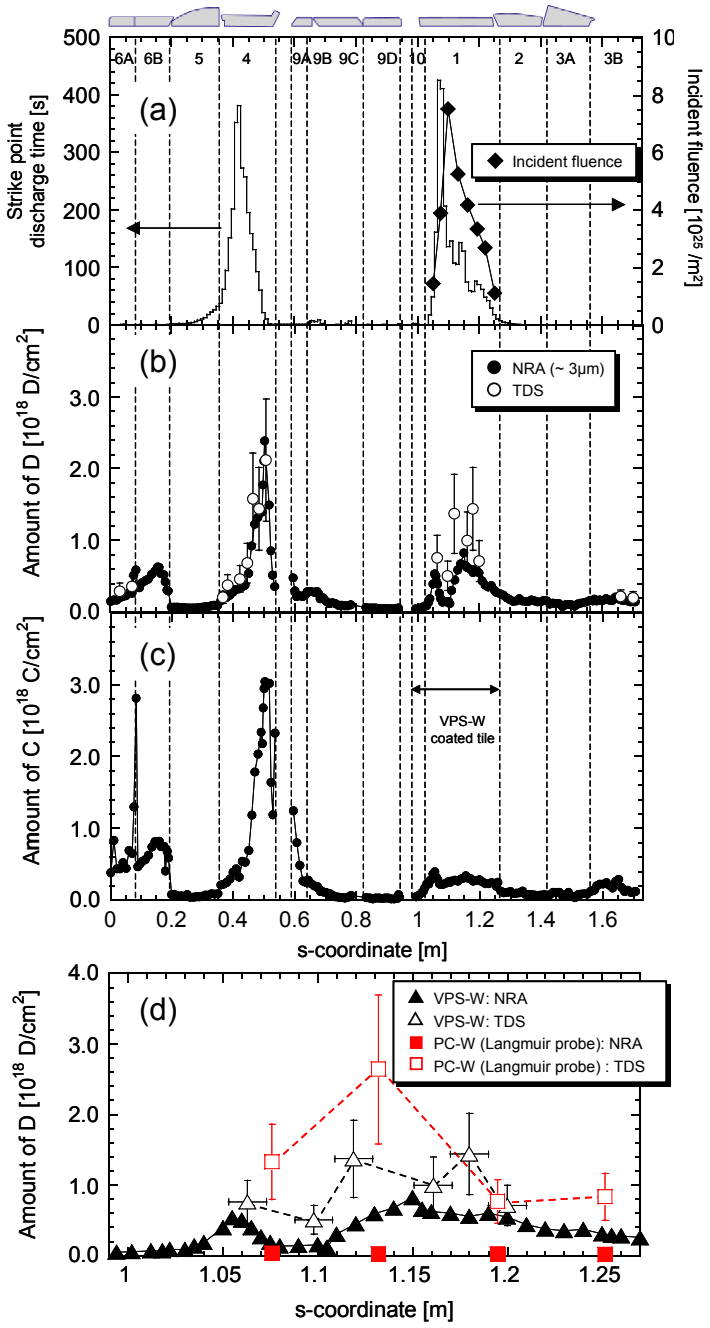

Figure 2. (a) Strike point position distribution during the 2007 campaign together with incident fluences on the outer divertor region measured by each Langmuir probe, (b) amount of D determined by NRA (2.5 MeV $^3He^+$: depth information ~ 3 μm) and TDS, and (c) amount of C determined by NRA. (d) Comparison of the amounts of D trapped in VPS-W and PC-W Langmuir probes in the outer divertor (tile No. 1).

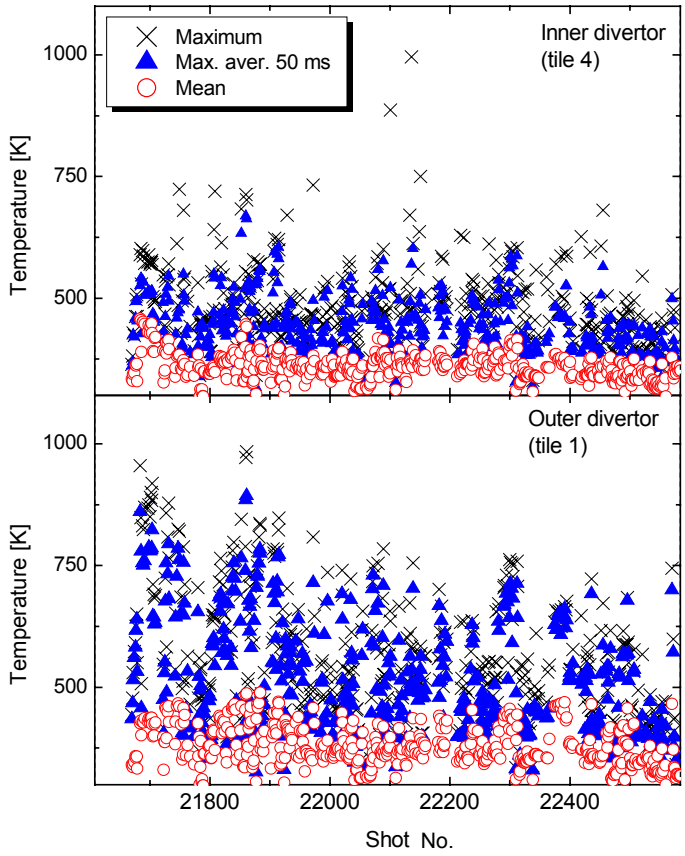

Figure 3: Surface temperature history of the inner and outer strike point tiles during the 2007 discharge campaign. Crosses: maximum surface temperature during a discharge. Triangles: maximum average surface temperature (averaged over 50 ms) during a discharge. Circles: mean surface temperature averaged over the whole tile and the whole discharge.

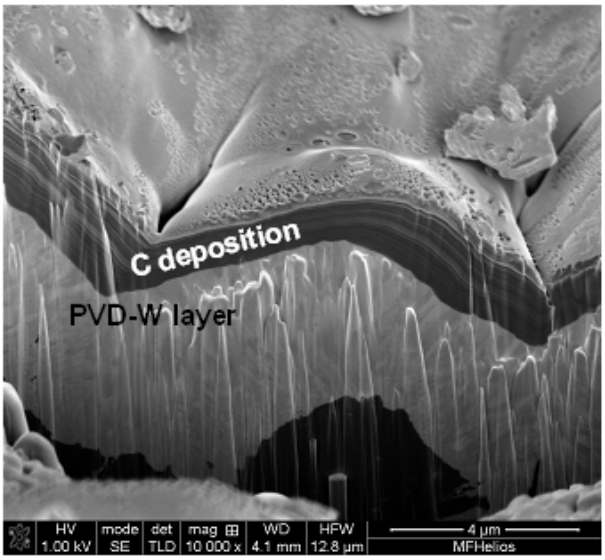

Figure 4. SEM image of the cross-section of a deposited carbon layer on the PVD-W coated tile (s ~ 0.5 m: private flux region). The cross section was prepared by cutting with FIB.

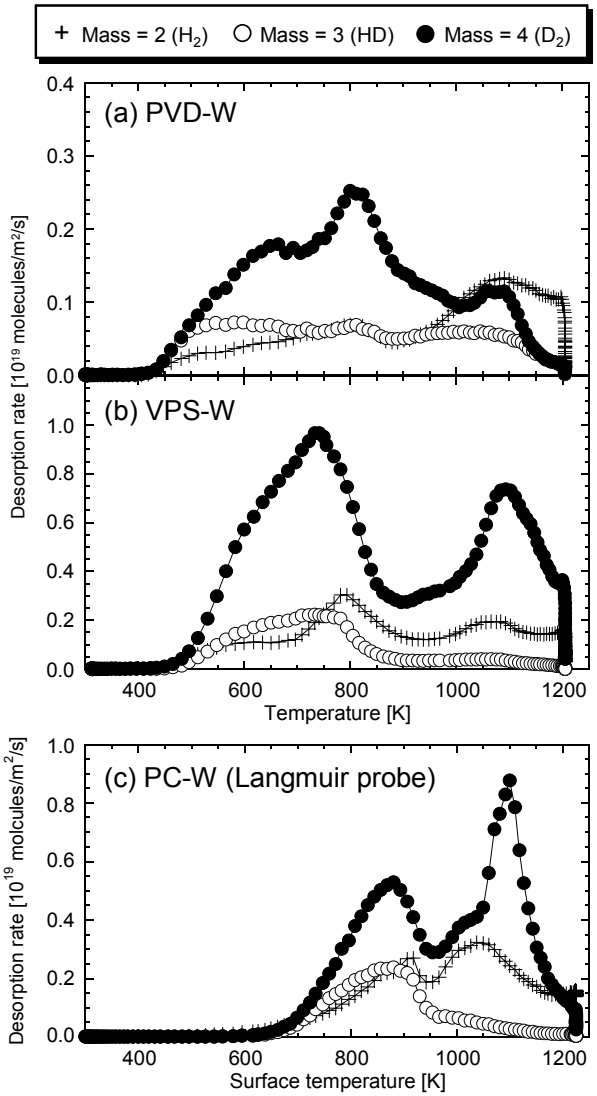

Figure 5. Typical TDS profiles of (a) PVD-W sample from the inner divertor (s ~ 0.38 m), (b) VPS-W sample from the outer divertor (s ~ 1.195 m) and (c) PC-W (Langmuir probe: s ~ 1.195 m). The heating rate of TDS was ~ 0.5 K/s. Note that the temperature for Langmuir probe samples is given as "surface temperature" indicating the temperature measured by a thermocouple, which was attached to the probe surface.

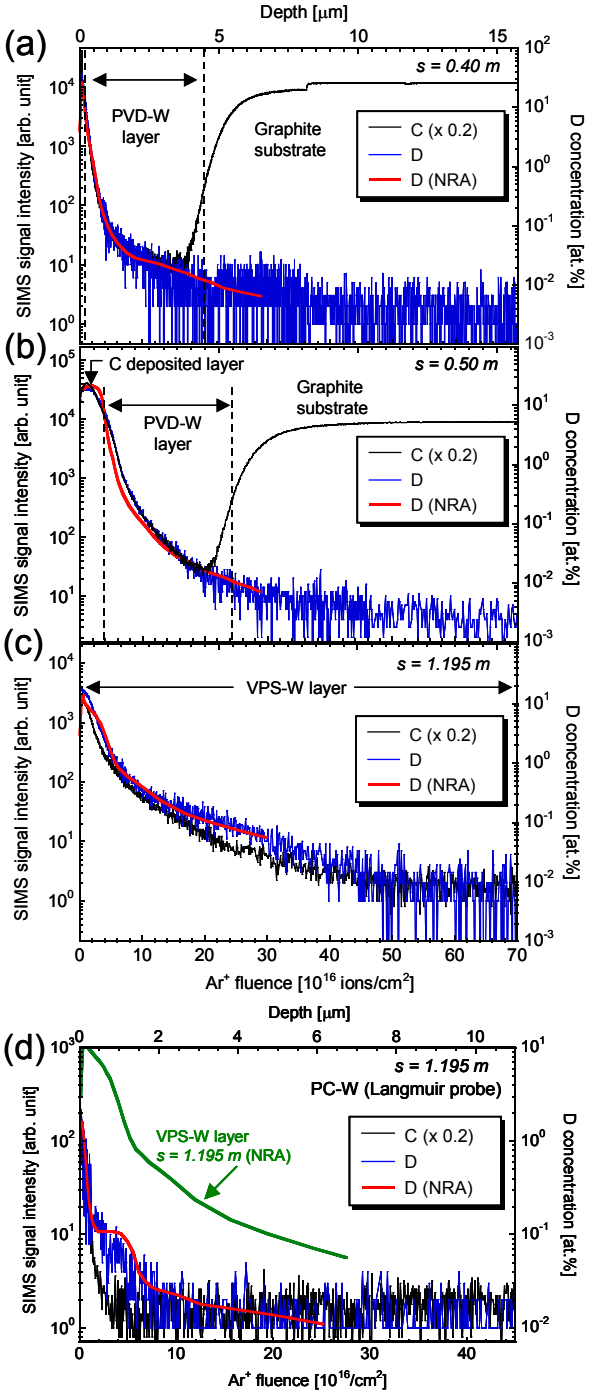

Figure 6. Depth profiles of D and C measured by SIMS together with D depth profile determined by NRA. (a) PVD-W sample from the inner divertor (s ~ 0.40 m), (b) PVD-W sample with deposited C layer from the inner divertor (s ~ 0.50 m, see also Fig. 2), (c) VPS-W sample from the outer divertor (s ~ 1.195 m) and (d) PC-W Langmuir probe sample (s ~ 1.195 m).

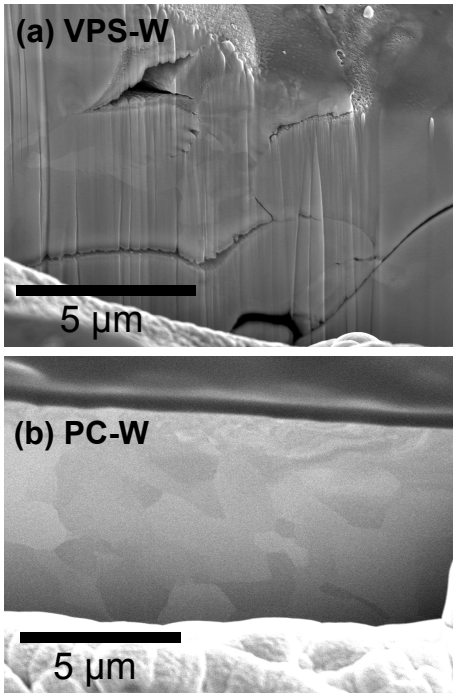

Figure 7. SEM images of FIB cross-sections of (a) VPS-W layer and (b) PC-W (Langmuir probe). In both pictures the additional structure at the bottom side is the surface structure in front of the trench cut out by FIB.

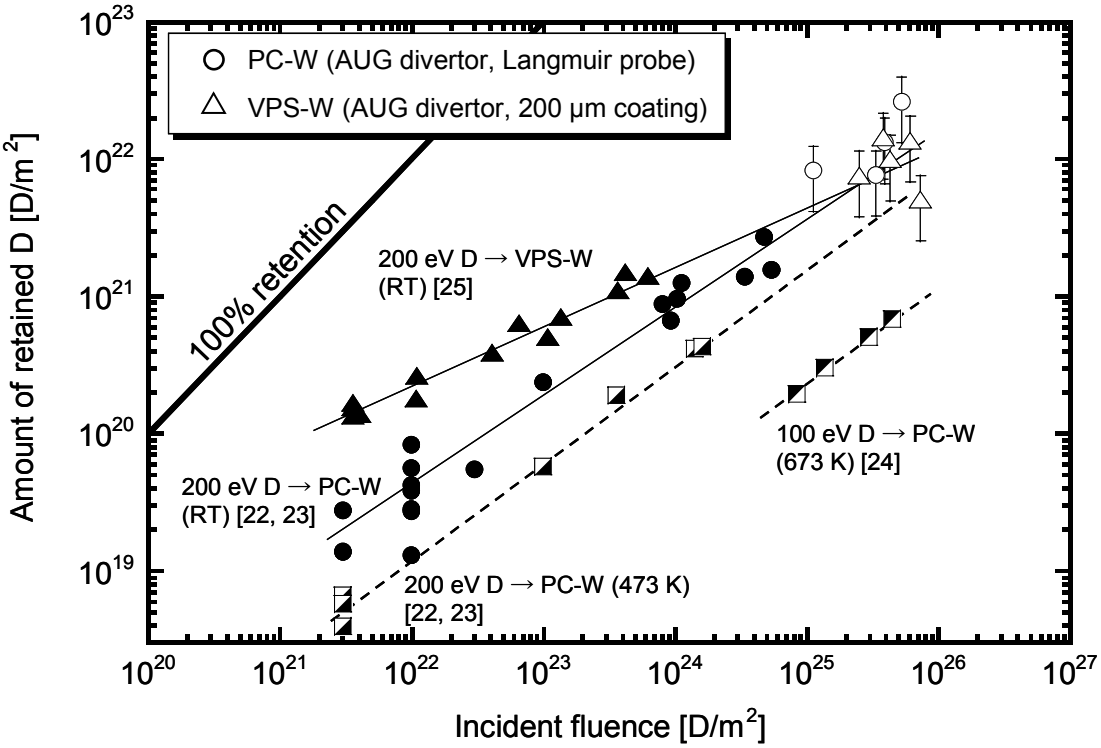

Figure 8. Comparison of the fluence dependences between AUG samples (PC-W from Langmuir probes and VPS-W from the outer target tiles) and literature data.

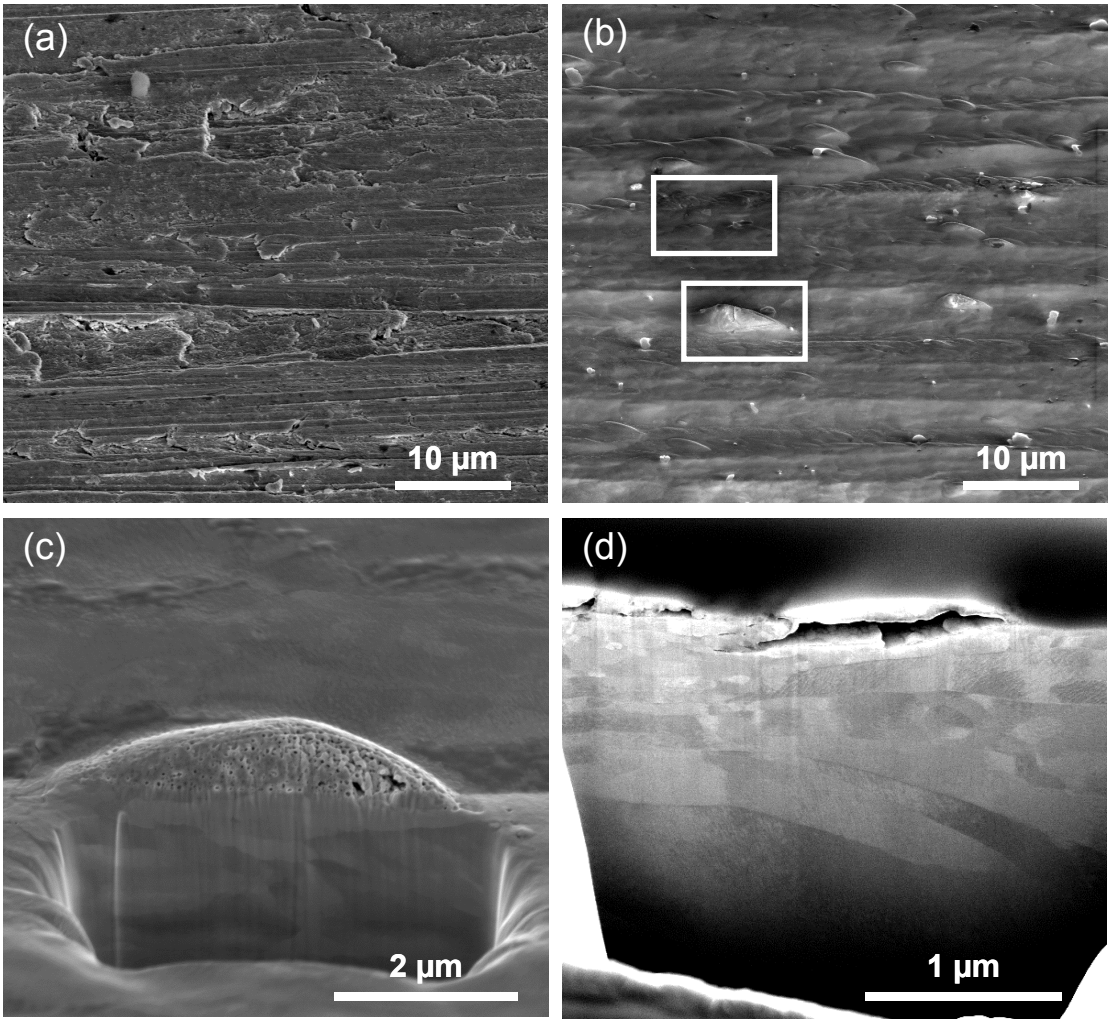

Figure. 9: SEM images of the PC-W surface (a) unexposed and (b, c, d) after plasma exposure. The slight blackening of the marked areas in (b) are caused by the chemical composition analysis of these areas; (c) FIB cross-section through a blister-like structure with foam-like morphology and without a large cavity below; (d) FIB cross-section through cavities created by machining (the surface was coated with a carbon coating before the FIB process).

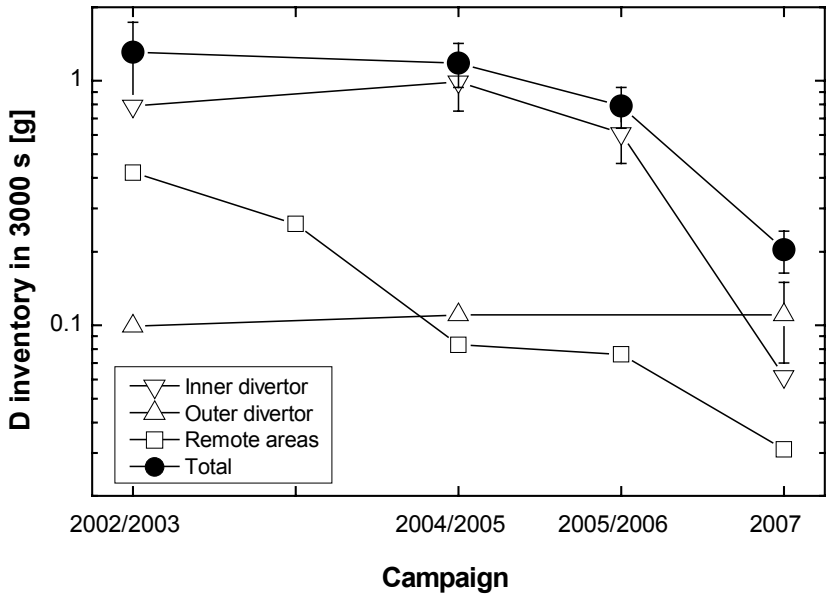

Figure 10. D inventory in the divertor and in remote areas of ASDEX Upgrade from 2002/2003 to 2007.

References

[1] Aymar R, Babaraschi P and Shimomura Y 2002 *Plasma Phys. Control. Fusion* **44** 519

[2] Federici G. *et al* 1999 *J. Nucl. Mater*. **266-269** 14

[3] Janeschitz G *et al* 2000 *Nucl. Fusion* **40** 1197

[4] Bolt H *et al* 2004 *J. Nucl. Mater.* **329-333** 66

[5] Roth J *et al* 2008 *Plasma Phys. Control. Fusion* **50** No.10 103001

[6] Neu R *et al* 2007 *J. Nucl. Mater.* **363-365** 52

[7] Deschka S *et al* 1996 *J. Nucl. Mater.* **233-237** 645

[8] Maier H *et al* 2001 *Surface and Coating Tech.* **142-144** 733

[9] Neu R. *et al*., *Fusion Eng. Des.* **65** (2003) 367

[10] Herrmann A 1996 *Optical surface temperature measurement*, in *Diagnostics for Experimental Thermonuclear Fusion Reactors*, P.E. Stott, G. Gorini, and E. Sindoni, Editors. Plenum Press, New York and London

[11] Herrmann A *et al* 1995 *Plasma Phys. Control. Fusion* **37** 17

[12] Mayer M *et al* 2007 *Nucl. Fusion* **47** 1607

[13] Herrmann A, Greuner H, Neu R 2009 "Experiences with tungsten coatings in high heat flux tests and under plasma load in ASDEX Upgrade" *Phys. Scr.* **T138** at press

[14] Alimov V Kh, Mayer M, Roth J 2005 *Nucl. Instr. and Meth. in Phys. Res. B* **234** 169

[15] Mayer M *et al* 2009 *Nucl. Instr. and Meth. in Phys. Res.* B **267** 506

[16] Mayer M 1997 SIMNRA User's Guide, *IPP Report 9/113*, Max-Planck-Institut für Plasmaphysik, Garching, Germany

[17] Salançon E *et al* 2008 *J. Nucl. Mater.* **376** 160

[18] Mayer M *et al* 2009 *J. Nucl. Mater.* **390-391** 538

[19] Herrmann A *et al* 2009 *J. Nucl. Mater*. **390-391** 747

[20] Droste S *et al* 2008 *Plasma Phys. Control. Fusion* **50** 015006

[21] Kreter A. *et al* 2008 *Plasma Phys. Control. Fusion* **50** 095008

[22] Ogorodnikova O V, Roth J and Mayer M 2003 *J. Nucl. Mater.* **313-316** 469

[23] Ogorodnikova O V, Roth J and Mayer M 2008 *J. Appl. Phys.* **103** 034902

[24] Venhaus T *et al* 2001 *J. Nucl. Mater.* **290-293** 505

[25] Golubeva A V *et al* 2006 "Hydrogen retention in plasma-sprayed tungsten" In Hydrogen in Matter: *A Collection from the Papers Presented at the 2nd International Symposium on Hydrogen in Matter; ISOHIM* vol. 837 of AIP Conference Proceedings, American Insitute of Physics

[26] Fransens J R *et al* 1991 *J. Phys. Condens. Mater.* **3** 9871

[27] Eleveld H van Veen A 1992 *J. Nucl. Mater*. **191-194** 433

[28] Poon M, Haasz A A, Davis J. W. 2008 *J. Nucl. Mater*. **374** 390

[29] Frauenfelder R 1969 *J. Vac. Sci. Technol.* **6** 388

[30] Zakharov A P, Sharapov V M, Babad-Zakhryapin A A, 1979 *Proc. 1st. Int. Congress on Hydrogen in Metals*, Paris, France 217

[31] Krieger K. *et al* 2007 *J. Nucl. Mater.* **363-365** 870

[32] García-Rosales C *et al* 1996 *J. Nucl. Mater.* **233-237** 803

[33] Mayer M *et al* 2007 *J. Nucl. Mater.* **363-365** 101

[34] Scherzer B M U 1983 in "Sputtering by Particle Bombarmend II", *Ed. R. Behrisch, Springer-Verlag* 271

[35] Shu W M *et al* 2009 *J. Nucl. Mater.* **390-391** 1017

[36] Lindig S *et al* 2009 "Subsurface morphology changes due to deuterium bombardment of tungsten" *Phys. Scr.* **T138** at press

[37] Radel R F, Kulcinski G L 2007 *J. Nucl. Mater.* **367-370** 434

[38] Sharafat S *et al* 2009 *J. Nucl. Mater.* **389** 203

[39] Mayer M *et al* 2009 "Tungsten erosion and redeposition in the all-tungsten divertor of ASDEX upgrade" *Phys. Scr.* **T138** at press